Belt–zone contrasts in vertical motions and cloud structure in Jupiter's troposphere

João M. Mendonça[a,b], Tapio Schneider[b], Junjun Liu[b,c]

[a] *National Space Institute, Technical University of Denmark, Elektrovej, 2800 Kgs. Lyngby, Denmark*
[b] *California Institute of Technology, Pasadena, CA 91125, USA*
[c] *Space Science Institute, Boulder, CO 80301, USA*

Abstract

The eddy fluxes of angular momentum in Jupiter's upper troposphere are known to converge in prograde jets and diverge in retrograde jets. Away from the equator, this implies convergence of the Eulerian mean meridional flow in zones (anticyclonic shear) and divergence in belts (cyclonic shear). It indicates lower tropospheric downwelling in zones and upwelling in belts because the mean meridional circulation almost certainly closes at depth. Yet the observed banded structure of Jupiter's clouds and hazes suggests that there is upwelling in the brighter zones and downwelling in the darker belts. Here, we show that this apparent contradiction can be resolved by considering not the Eulerian but the transformed Eulerian mean circulation, which includes a Stokes drift owing to eddies and is a better approximation of the Lagrangian mean transport of tracers such as ammonia. The potential vorticity structure inferred from observations paired with mixing length arguments suggests that there is transformed Eulerian mean upwelling in zones

*Corresponding authors emails: joao.mendonca@space.dtu.dk, tapio@caltech.edu

and downwelling in belts. Simulations with a global circulation model of Jupiter's upper atmosphere demonstrate the plausibility of these inferences and allow us to speculate on the band structure at deeper levels.

Keywords: Atmospheres, dynamics, Jupiter, atmosphere, Jovian planets, Meteorology

---

1. Introduction

Observations of the structure of clouds and hazes and of turbulent momentum fluxes lead to apparently conflicting accounts of vertical motion in Jupiter's troposphere. On the one hand, the banded structure of Jupiter's clouds and hazes suggests that there is upwelling in the brighter zones and downwelling in the darker belts. (Zones are latitude bands of anticyclonic meridional shear of the zonal wind, and belts are latitude bands of cyclonic shear; see Fig. 1a). Upwelling in the zones is thought to lead to condensation of ammonia into relatively bright ice clouds in the upper troposphere; downwelling in the belts is thought to suppress ammonia ice cloud formation, revealing darker clouds and hazes at greater depth (e.g., Smith et al., 1979; Gierasch et al., 1986; Carlson et al., 1994; Porco et al., 2003; West et al., 2004).

On the other hand, momentum fluxes associated with large-scale (& 1000 km) eddies suggest the opposite sense of vertical motion in zones and belts. Eddy momentum fluxes in the upper troposphere generally converge in prograde zonal jets and diverge in retrograde jets (Ingersoll et al., 1981; Salyk et al., 2006); that is, they converge near the equatorward edges of the belts and diverge near their poleward edges (Fig. 1b, dashed blue line).

But outside the equatorial region, where the Rossby number is small, the dominant balance in the zonal momentum equation is

$$f\bar{v} \quad S; \tag{1}$$

that is, the Coriolis acceleration (Coriolis parameter f) of the Eulerian mean meridional flow $\bar{v}$ balances the horizontal eddy momentum flux divergence S to leading order. Hence, the eddy momentum flux convergence ($S <$ 0) observed in prograde jets in the upper troposphere implies equatorward Eulerian mean meridional flow $\bar{v}$; the eddy momentum flux divergence ($S >$ 0) observed in retrograde jets implies poleward Eulerian mean meridional flow $\bar{v}$ (Fig. 1b, orange line). This leads to convergence of the Eulerian mean meridional flow in zones and divergence in belts, suggesting lower-tropospheric downwelling in zones and upwelling in belts (Fig. 1d, dashed blue line) because the Eulerian mean meridional circulation almost certainly closes at depth and not above the upper-tropospheric clouds from which the eddy momentum fluxes are inferred (Haynes et al., 1991; Schneider and Liu, 2009; Liu and Schneider, 2010; see section 2 below for a review of the arguments). Thus, there exists an apparent contradiction between inferences drawn from dynamical observations and from the structure of clouds and hazes.

Here, we show that this apparent contradiction can be resolved if one does not consider the Eulerian mean flow but an approximately Lagrangian mean flow. In the mean, tracers in turbulent flows are generally not advected by the Eulerian mean flow but by a Lagrangian mean flow, which contains a contribution owing to Stokes drift. Andrews and McIntyre (1976, 1978) showed that the Lagrangian mean flow advecting nearly conserved tracers

can be approximated by adding an eddy contribution representing the Stokes drift to the Eulerian mean flow. We will show with scaling arguments and with numerical simulations that once the Stokes drift is taken into account, observations of Jupiter's dynamics are consistent with the upwelling in zones and downwelling in belts suggested by the structure of clouds and hazes. The vertical motion is primarily accomplished by turbulent eddies, not the Eulerian mean flow.

2. Scaling arguments based on zonal momentum balance

2.1. Eulerian mean flow

The zonal momentum (or angular momentum) balance in Jupiter's troposphere is relatively simple because the Rossby number Ro = $U/(fL)$ is small. With horizontal velocity scale U $10\,\mathrm{m\,s^{-1}}$ (appropriate outside the equatorial region, see Salyk et al., 2006), scale of horizontal flow variations L 2000 km (Fig. 1a), and Coriolis parameter $f = 2\Omega\sin$ (planetary rotation rate $\Omega = 1.76 \quad 10^{-4}$), we have Ro < 0.2 outside 4 latitude. Hence, the flow is geostrophic to leading order. Additionally, variations of the Coriolis parameter f over the flow scale L are small: with $= a^{-1}\partial f$ (Jupiter radius a), we have $L/f < 0.2$ outside 8 latitude. It follows that outside the equatorial jet (Fig. 1a), the leading-order geostrophic flow is approximately non-divergent, and vertical advection terms can be neglected in the zonal momentum balance. In a statistically steady state—a good approximation for Jupiter, as evidenced by the weak zonal-flow variations between the Voyager and Cassini observations (Porco et al., 2003)—the

Eulerian mean zonal momentum equation thus is to leading order

$$f\bar{v} \quad S \quad \bar{X}: \tag{2}$$

Here,

$$S = \frac{1}{a\cos^2} \frac{@}{@}(\overline{u'v'}\cos^2 \quad) \tag{3}$$

is the horizontal eddy (angular) momentum flux divergence (zonal velocity u and meridional velocity v). Vertical momentum fluxes do not enter to leading order because the horizontal flow is approximately geostrophic and non-divergent (e.g., Andrews et al., 1987). Zonal accelerations owing to molecular diffusion and/or smaller-scale turbulent Reynolds stresses are subsumed in X. Overbars denote a temporal and zonal mean at constant pressure; primes denote deviations therefrom. If we neglect $\bar{X}$—molecular diffusion is negligible, and there is no evidence smaller-scale turbulent Reynolds stresses are important at leading order in Jupiter's (or Earth's) free troposphere—the zonal momentum balance (2) reduces to Eq. (1) in the introduction. Because the mean meridional flow $\bar{v}$ is entirely ageostrophic (the geostrophic meridional flow vanishes in the zonal mean), it is weaker by a factor $O(\mathrm{Ro})$ than the approximately geostrophic mean zonal flow $\bar{u}$. Hence, in midlatitudes where zonal flow speeds are of order $U \quad 10\,\mathrm{m\,s}^{-1}$ but $\mathrm{Ro} \;.\; 0{:}02$, $\bar{v}$ can at most be expected to be $O(0{:}2\,\mathrm{m\,s}^{-1})$.

The mean meridional flow $\bar{v}$ on Jupiter is too weak for us to be able to infer its meridional structure reliably from observations (Salyk et al., 2006). However, the eddy momentum flux divergence S can be inferred by tracking observed cloud features because it involves covariation between the approximately geostrophic, and hence much stronger, eddy velocities u' and v'.

While there are quantitative uncertainties, its qualitative structure is unambiguous (Salyk et al., 2006): at the level of the visible clouds and hazes in the upper troposphere, eddy momentum fluxes converge in prograde jets and diverge in retrograde jets (Fig. 1b). In Fig. 1b, we used the observed eddy momentum flux divergence S (dashed blue line) to construct the implied mean meridional flow $\bar{v} = S/f$ (orange line). The thus constructed mean meridional flow is indeed weak, $O(0.03\,\mathrm{m\,s^{-1}})$, which accounts for the difficulties of observing it directly. However, it is evident that, as stated in the introduction, the Eulerian mean meridional flow $\bar{v}$ implied by the eddy momentum flux divergence in the upper troposphere converges in zones [$\partial(\bar{v}\cos\phi)/\partial\phi < 0$] and diverges in belts [$\partial(\bar{v}\cos\phi)/\partial\phi > 0$].

Upper-tropospheric convergence of the Eulerian mean meridional flow implies mean downwelling, and divergence implies mean upwelling in the underlying lower troposphere because, as on Earth, the mean meridional overturning circulation almost certainly closes not in the upper atmosphere (upper troposphere and above) but at depth. The reasons for this are rooted in the mass and angular momentum balances: Integrated over surfaces of constant mean absolute angular momentum per unit mass, these balances demand that in a statistically steady state, (i) the mean mass circulation closes, and (ii) any angular momentum flux divergence/convergence on a mean angular momentum surface is balanced by drag on a retrograde/prograde zonal flow or by compensating angular momentum flux convergence/divergence somewhere else on the angular momentum surface. Otherwise, the mean distributions of mass and angular momentum would shift, in violation of the statistically steady state assumption (e.g., Haynes et al., 1991; Schneider and

Liu, 2009; Liu and Schneider, 2010). If angular momentum fluxes compensating those observed in the upper troposphere occurred at yet higher levels in the atmosphere, they would have to be accomplished by eddies with velocities similar to or greater than those seen in the upper troposphere because of the exponential decrease of density with height. No model has produced such eddy fluxes, and they have not been observed. Moreover, there is no viable mechanism to dissipate angular momentum in the upper atmosphere by drag on a zonal flow because the atmosphere cannot exert a torque on outer space. Therefore, the Eulerian mean mass circulation implied by the observed eddy momentum fluxes almost certainly closes at depth, according to the principle of "downward control" of atmospheric overturning circulations (Haynes et al., 1991). At depth, it can close, for example, in a layer of magnetohydrodynamic (MHD) drag where the atmosphere becomes electrically conducting (Liu et al., 2008; Schneider and Liu, 2009; Liu and Schneider, 2010; Liu et al., 2013).

The conclusion appears inevitable, then, that to leading order, there is Eulerian mean downwelling in zones and upwelling in belts in Jupiter's lower troposphere. Assuming that the upper branch of the mean meridional overturning circulation is distributed over a layer with a thickness comparable to or greater than the density scale height H, a rough estimate of the Eulerian mean vertical velocity below this layer is $\bar{w} \quad (H/2)\,\mathrm{div}\,\bar{\mathbf{v}} = (H/2)@\ (\bar{v}\cos\ )/(a\cos\ )$. This estimate for $H = 20\,\mathrm{km}$ (appropriate for Jupiter's upper troposphere) is shown in Fig. 1d (dashed blue line). The vertical velocity is $O(10^{-4}\,\mathrm{m\,s^{-1}})$ and clearly is negative (downwelling) in zones and positive (upwelling) in belts. This apparently contradicts the inferences

from the structure of clouds and hazes. The contradiction is resolved by considering an approximately Lagrangian mean flow.

2.2. Transformed Eulerian mean flow

Andrews and McIntyre (1976, 1978) showed that the Lagrangian mean flow advecting nearly conserved tracers can be approximated by the transformed Eulerian mean (TEM) flow. In a statistically steady state under quasigeostrophic scaling (which includes, in addition to the scaling assumptions of the previous section, the assumption that the thermal stratification is stable and relatively constant), the TEM flow has meridional and vertical components

$$\bar{v} = \bar{v} - \frac{\partial}{\partial p}\left(\frac{\overline{v'\theta'}}{\partial_p \bar{\theta}}\right) \tag{4}$$

and

$$\bar{\omega} = \bar{\omega} + \frac{1}{a\cos\phi}\frac{\partial}{\partial \phi}\left(\frac{\overline{v'\theta'}}{\partial_p \bar{\theta}}\cos\phi\right) : \tag{5}$$

Here, $\omega = Dp/Dt$ is the vertical velocity in pressure coordinates, and θ is the potential temperature. The terms involving the meridional eddy flux of potential temperature $\overline{v'\theta'}$ represent approximately the Stokes drift. Adding the Stokes drift term on both sides of the Eulerian mean zonal momentum equation (1) gives the TEM zonal momentum equation,

$$f\bar{v} = S - f\frac{\partial}{\partial p}\left(\frac{\overline{v'\theta'}}{\partial_p \bar{\theta}}\right) = \frac{1}{a\cos\phi}\nabla_p \cdot \mathbf{F} \tag{6}$$

where we have written the right-hand side in terms of the divergence ($\nabla_p \cdot$) of the Eliassen-Palm flux $\mathbf{F} = (F_\phi, F_p)$ in the latitude-pressure plane (Edmon et al., 1980), with

$$F_\phi = -\overline{u'v'}\, a\cos\phi \quad \text{and} \quad F_p = f\frac{\overline{v'\theta'}}{\partial_p \bar{\theta}}\, a\cos\phi : \tag{7}$$

The Eliassen-Palm flux is, under certain conditions, the flux of pseudo-momentum (or wave activity), which is conserved by eddies (rather than by the total flow consisting of eddies and the Eulerian mean); hence, it is convenient in reasoning about how eddies interact with the mean flow and lead to mean transport of tracers (e.g., Andrews, 1987). The Eliassen-Palm flux is related to the eddy flux of quasigeostrophic potential vorticity,

$$q = f + \quad + f \frac{@}{@p} \quad \overline{\quad =} \quad ; \tag{8}$$

with relative vorticity , by the Taylor-Bretherton identity (Taylor, 1915; Bretherton, 1966; Edmon et al., 1980)

$$\frac{1}{a \cos} \, r_p \quad \mathbf{F} = \overline{v^{\prime} q^{\prime}} : \tag{9}$$

Combining the relations (6) and (9) gives the well-known result that the TEM meridional flow is determined by the eddy flux of potential vorticity, which is conserved in adiabatic and frictionless eddy fluctuations (e.g., Andrews et al., 1987):

$$f \bar{v} \;=\; \overline{v^{\prime} q^{\prime}} : \tag{10}$$

The TEM vertical flow follows by continuity, $r_p \quad (\bar{v} \; ; \; \dot{} \;) = 0$. These relations can be generalized to settings when quasigeostrophic scaling does not hold or when tracers are not nearly conserved (e.g., Andrews, 1983; Tung, 1986; Andrews et al., 1987; Koh and Plumb, 2004; Schneider, 2005; Plumb and Ferrari, 2005). However, this is not necessary for a discussion of nearly conserved tracers in Jupiter's upper troposphere (above 400 mbar), which is stably stratified and, for now, is our focus here.

The relation (10) allows us to derive a better approximation of the mean flow advecting tracers such as ammonia in Jupiter's upper troposphere. Un-

fortunately, the potential temperature flux contained in the potential vorticity or Eliassen-Palm flux (7) has not been directly measured. But as a first scaling estimate, we can assume the quasigeostrophic potential vorticity flux is downgradient and diffusive,

$$\overline{v^{\prime}q^{\prime}} \qquad D@_y\bar{q}; \tag{11}$$

where $y = a$ and $D > 0$ is an eddy diffusivity. Unlike diffusive approximations for quantities such as angular momentum, which is not conserved by eddies, a diffusive approximation for quasigeostrophic potential vorticity is justifiable for two reasons (Corrsin, 1974; Rhines and Holland, 1979; Plumb, 1979; Held, 2000): (i) quasigeostrophic potential vorticity is only weakly nonconserved in the essentially frictionless and nearly adiabatic (rapid compared with radiative timescales) eddy fluctuations in Jupiter's upper troposphere; and (ii) the mean quasigeostrophic potential vorticity primarily varies on meridional scales that are large compared with eddy length scales (Read et al., 2006). These two assumptions may not be satisfied accurately everywhere. For example, the mean quasigeostrophic potential vorticity has variations on the meridional scale of the zonal jets, which is similar to the eddy length scale; see below. But the diffusive approximation is a useful starting point for scaling arguments (e.g., Held, 1999; Held and Schneider, 1999; Schneider, 2004; Schneider and Walker, 2006).

We assume the eddy diffusivity D varies at most on scales that are large compared with meridional flow scales so that the diffusive approximation is justifiable. Then, the relation (10) with the diffusive closure (11) implies

that the TEM meridional flow,

$$\bar{v} \qquad \frac{D}{f}\partial_y \bar{q}; \tag{12}$$

is strongly poleward where the quasigeostrophic potential vorticity gradient $\partial_y \bar{q}$ is strongly positive; it is more weakly poleward or equatorward where $\partial_y \bar{q}$ is more weakly positive or negative. Now, the quasigeostrophic potential vorticity gradient $\partial_y \bar{q}$ in Jupiter's upper troposphere at least above 270 mbar is dominated by the barotropic component $\partial_y \bar{q} \qquad + \partial_y \bar{}$, the gradient of the absolute vorticity $f +$; the stretching term only modifies $\partial_y \bar{q}$ by 10% (Read et al., 2006). Hence, we ignore the stretching term here, although its contribution is more likely to be significant at lower levels, where the thermal stratification is close to neutral. The absolute vorticity gradient in the upper troposphere is locally enhanced in the cores of prograde jets (where $\partial_y \bar{} > 0$ because the zonal flow curvature is negative); it is reduced in the cores of retrograde jets (where $\partial_y \bar{} < 0$ because the zonal flow curvature is positive). The planetary vorticity gradient varies only on scales larger than the meridional jet scales and hence does not contribute substantially to modulations of the absolute vorticity gradient on the scales of zones and belts (Fig. 1c). It follows that the TEM meridional flow $\bar{v}$ can be expected to be relatively strongly poleward in prograde jets and more weakly poleward or even equatorward in retrograde jets. This leads to convergence in belts and divergence in zones. It resembles the ad hoc suggestion by Gierasch et al. (1986), for a TEM meridional flow that alternates between prograde and retrograde jets. The distinction between that work and our work is that the TEM meridional flow we suggest does not need to change sign between jets but may be predominantly poleward throughout the upper troposphere,

only with strength variations between jets.

To be concrete, let us assume the diffusivity is constant and can be estimated from the meridional eddy velocity scale $V \sim 3\,\mathrm{m\,s^{-1}}$ (Salyk et al., 2006) and the meridional eddy length $L \sim 2000\,\mathrm{km}$, so that $D \sim VL \sim 6 \times 10^6\,\mathrm{m\,s^{-2}}$. Figure 1c shows the TEM meridional flow (orange line) that results when the quasigeostrophic potential vorticity gradient $\partial_y \bar{q}$ is approximated by the absolute vorticity gradient $\partial_y(f + \bar{\zeta})$ (dashed blue line) obtained from the observed zonal flow in Fig. 1a (Salyk et al., 2006). The resulting TEM meridional flow is of order $\bar{v} \sim D/f \sim 0.3\,\mathrm{m\,s^{-1}}$ in midlatitudes—an order of magnitude stronger than the Eulerian mean meridional flow. As the absolute vorticity gradient is generally positive, except in some retrograde jets (Ingersoll et al., 1981; Salyk et al., 2006), the TEM meridional flow likewise is generally poleward. It is clear from Fig. 1c that the TEM meridional flow implied by the diffusive potential vorticity flux closure converges in belts [$\partial(\bar{v}\cos\phi) < 0$] and diverges in zones [$\partial(\bar{v}\cos\phi) > 0$]. Because the TEM mass circulation almost certainly closes at depth for reasons analogous to those for the Eulerian mean circulation (with potential vorticity fluxes replacing angular momentum fluxes in the arguments), this suggests that in the underlying lower troposphere, there is TEM downwelling in belts and upwelling in zones. The rough estimate $\bar{w} \sim (H/2)\,\mathrm{div}\,\bar{v}$ of the TEM vertical velocity below the upper branch of the TEM mass circulation is shown in Fig. 1d (orange line). This TEM vertical velocity is of order $O(10^{-3}\,\mathrm{m\,s^{-1}})$—an order of magnitude stronger than the corresponding Eulerian mean vertical velocity.[1] It clearly is positive (upwelling) in zones and

[1]This TEM vertical velocity is about an order of magnitude stronger than the TEM

negative (downwelling) in belts.

Thus, the TEM circulation inferred by the diffusive potential vorticity flux closure is much stronger and has the opposite direction of vertical motion than the Eulerian mean circulation. It is qualitatively consistent with the observed structure of clouds and hazes (Fig. 1d). Based on our scaling arguments, barotropic variations of the quasigeostrophic potential vorticity gradient are responsible for the jet-to-jet variations of potential vorticity fluxes. These meridionally varying potential vorticity fluxes, in turn, are associated with a TEM meridional flow that is more strongly poleward in prograde jets and less strongly poleward or even equatorward in retrograde jets, and so, at deeper levels, drives upwelling in zones and downwelling in belts. While the meridional flow in the Eulerian mean circulation is associated with eddy momentum flux divergence S, or with the barotropic component of the potential vorticity flux, the much greater strength of the TEM circulation implies that the baroclinic component of the potential vorticity flux, involving the meridional heat flux in Eq. (6), dominates. The baroclinic component of the potential vorticity flux is associated with an eddy mass flux along isentropes (Schneider, 2005; Vallis, 2006, chapter 7.3), which represents a Stokes drift and accomplishes the TEM circulation. Note that there is no contradiction in assuming that the *mean* potential vorticity gradient in the

vertical velocity around 100 mbar estimated from radiative transfer calculations and observed properties of Jupiter's upper atmosphere (West et al., 1992; Moreno and Sedano, 1997). There is no contradiction, however, as our estimates apply to the layer of the visible cloud tops (below 270 mbar), and the TEM vertical velocity can be expected to decrease upward toward the tropopause (at 100 mbar).

upper troposphere is dominated by its barotropic component, whereas the *eddy* flux of potential vorticity is predominantly baroclinic.

3. Demonstration with global circulation model

We demonstrate the validity of the scaling arguments with simulation results from the global circulation model (GCM) of Jupiter's upper atmosphere that was developed and presented in Young et al. (2019a,b)[2]. The Jupiter GCM is based on the MITgcm (Marshall et al., 1997b,a; Adcroft et al., 2004), with a latitude-longitude grid configuration and a finite-difference dynamical core. The GCM has an artificial lower boundary at 18 bar, which is necessary to make it computationally feasible to resolve large-scale eddies in the upper atmosphere while remaining consistent with Jupiter's observed energetics (Young et al., 2019a). At the lower boundary, a linear drag mimics, in a simplified way, the MHD drag on the flow that occurs in Jupiter at much greater depth (Liu et al., 2008, 2013). Additionally, a spatially uniform upwelling heat flux representing Jupiter's intrinsic heat flux is imposed. A semi-grey radiative transfer scheme, similar to that used in Schneider and Liu (2009), is utilized to represent radiative processes. To improve accuracy in the deepest layers with large optical depths, the radiation scheme utilizes an exponential dependence of the Planck function on optical depth for the thermal infrared radiation part. This approach was discussed in Fu and Liou (1993) and Mendonça et al. (2015). The absorbed solar radiative flux is $8.2\,\mathrm{W\,m^{-2}}$ in the global mean, and the imposed intrinsic heat flux at the

[2]The GCM data used in this work can be found in Young (2018): 10.5287/bodleian:PyYbbxpk2.

lower boundary amounts to 5.7 W m $^{-2}$ (Read et al., 2016). The Jupiter GCM also takes into account the effects of latent heat release in condensation of a water vapor tracer, as well as the physical manifestations of dry and moist convection (Zuchowski et al., 2009). To study the layered cloud structures in Jupiter (Zuchowski et al., 2009), the GCM allows the advection of H_2O, NH_3, and NH_4SH in gas and liquid form. The GCM uses Jupiter's planetary radius, rotation rates, and other physical parameters. Further details can be found in Young et al. (2019a,b).

The results from the Jupiter GCM were obtained using a horizontal spatial resolution of 0.7^o, which is necessary to resolve the first baroclinic Rossby radius and to simulate Jupiter's meteorology (Achterberg and Ingersoll, 1989; Vasavada and Showman, 2005; Read et al., 2006). The simulations were integrated over 130,000–150,000 Earth days. Long-time integration is required due to the slow thermal and dynamical adjustment of the deep atmosphere.

The GCM reproduces qualitatively many of the observed features of Jupiter's flow and temperature structure. For example, in the upper troposphere, it reproduces a prograde equatorial jet and weaker alternating retrograde and prograde off-equatorial jets (Fig. 2a, contours). Eddy momentum fluxes converge in prograde jets and diverge in retrograde jets (Fig. 2a, colors), with S reaching $O(10^{-5}\,\mathrm{m\,s^{-2}})$ in the upper troposphere—as observed on Jupiter (cf. Fig. 1b). As in the simulation, it must also be the case on Jupiter that the strongest eddy momentum flux convergence/divergence is confined to the upper troposphere because otherwise the kinetic energy transfer from eddies to the mean flow would exceed the energy available to drive the flow from the absorbed insolation and intrinsic heat fluxes (Schneider and Liu,

2009; Liu and Schneider, 2010). The simulated eddy momentum flux convergence and divergence pattern is consistent with baroclinic eddy generation that occurs preferentially in the baroclinically more unstable prograde jets (Schneider and Liu, 2009; Liu and Schneider, 2010, 2011; Young et al., 2019a). Additionally, the GCM reproduces the thermal structure of Jupiter's upper atmosphere, including a neutrally stratified lower troposphere overlaid by a stably stratified upper troposphere that is capped by a tropopause (Fig. 2b).

Thus, while this simulation does not replicate Jupiter's upper atmosphere exactly, it does reproduce its central dynamical balances as far as they are observed, and it can serve as a testbed to investigate the validity of the theoretical arguments we presented.

3.1. Upper-tropospheric dynamics

The Jupiter GCM produces a cloud band structure that resembles the one observed. Figure 3 shows the concentration of liquid NH_3 in the simulation, along with the belts and zones as identified by the relative vorticity field. As observed, higher concentrations of liquid NH_3 occur in zones with anticyclonic meridional shear of the zonal wind, while lower concentrations of liquid NH_3 are found in bands with cyclonic shear (Young et al., 2019b). The two hemispheres have a similar band structure, although they are not completely symmetrical. As observed, prograde jets are located on the equatorward flanks of the belts and retrograde jets on the poleward flanks. Each zonal structure is defined by its edges, which are located in regions where the vorticity changes sign (Figure 3). In these regions, there is a barrier to irreversible transport (Dritschel and McIntyre, 2008; Nikurashin et al., 2013). The transport barrier is not completely impermeable, and its per-

meability is reduced by wave erosion at all scales. The more clearly defined zonal structures of Jupiter's observed clouds indicate a reduced permeability across zonal jets compared with the model, possibly as a result of overly diffusive dynamics of the underresolved simulation.

Interestingly, as shown in Young et al. (2019b), the Jupiter simulations used here also produce an equatorial plume of NH_3 vapor similar to the one observed by Juno (Li et al., 2017). However, as explained in Young et al. (2019b), as the simulation progresses, more vapor is lifted in the tropical regions and spreads to higher latitudes due to turbulent mixing. In mid-latitudes, meridional circulation cells also slowly lift NH_3 vapor from the model's deeper layers, broadening the initial NH_3 plume latitudinally. The initial narrow equatorial plume produced in the simulation is a transient phenomenon that emphasises the role of the upwelling in the equatorial region (Young et al., 2019b).

3.1.1. Mean meridional circulation

To determine the validity of our theoretical arguments in the previous section, we plotted the meridional and vertical components of the Eulerian and transformed Eulerian mean circulations in Fig. 4. To make it compatible with the observations, the values plotted correspond to the upper cloud region in the GCM simulations (Fig. 3), above the weakly stratified region (Fig. 2b). The results correspond to a pressure level of approximately 200 mbar.[3] The Eulerian mean meridional flow (black lines) exhibits a simi-

[3]Note that the simulated atmosphere's weak static stability compromises the TEM flow's accuracy for depths greater than 300 mbar. At the 300 mbar pressure level, the

lar pattern to that inferred from observations in Fig. 1: convergence in zones and divergence in belts. By contrast, and in agreement with the theoretical arguments presented earlier, the TEM meridional flow (red line) generally exhibits convergence in belts and divergence in zones. However, the TEM meridional flow is of similar magnitude as the Eulerian mean flow component, unlike what we inferred from observations (Fig. 1b). The main differences between the simulations and observations lie in the magnitude of the meridional eddy velocity and the horizontal eddy momentum flux divergence S. The meridional eddy velocity has a magnitude in the simulations of around $1\,\mathrm{m\,s^{-1}}$, which is a factor of 3 smaller than our estimates based on the observations by Salyk et al. (2006). Observations also show a stronger eddy momentum flux divergence compared with the simulations at the 200-mbar pressure level. Fig. 2a shows a decrease in the horizontal eddy momentum flux divergence as the altitude increases from around the 400-mbar pressure level. However, the TEM flow is not computed for pressure levels deeper than 200 mbar because of the low static stability at deeper levels. Nonetheless, the results emphasize the importance of the horizontal eddy momentum flux divergence and meridional eddy velocity in interpreting TEM flow components, which is consistent between simulations and observations.

For the TEM vertical flow, it is important to highlight that the GCM simulations show, on average, a pattern that aligns with the scaling arguments from the previous section. Our results help to resolve the inconsistency in the contrasts of belt-zone vertical motions and cloud structure (Fletcher et al.,

impact of static stability on TEM flow becomes evident as $\bar{v}^*$ increases rapidly towards higher latitudes, where static stability decreases quasi-monotonically with latitude.

2020). The pattern of the TEM vertical flow is consistent with the convergence and divergence regions of the TEM meridional flow, with enhanced upwelling in zones (Fig. 4). The consistency with the scaling arguments and observations is stronger at the center of the bands. However, it becomes more complex near the band's edges, which show larger vertical wind shears. These wind shears might contribute to turbulent mixing between different band structures. This mixing is more pronounced in the simulations than in the observations, resulting in less confined belts/zones in the simulations compared to the observations. The magnitudes of the vertical flow in the TEM and Eulerian mean are similar in the simulation but weaker than the values inferred from observations. Such a trend is also seen in the meridional direction analysis, as described above.

4. Conclusions

The angular momentum balance provides powerful constraints based on already available observations. In this work, we used fundamental principles of the angular momentum balance, together with simple diffusive closures for potential vorticity fluxes, to physically constrain the atmospheric circulation in Jupiter's troposphere and reasoned how it extends to deeper levels. We resolved the apparent contradiction between the contrasts of belts and zones and vertical motion in Jupiter's troposphere by considering the transformed Eulerian mean (TEM) circulation to represent the Lagrangian mean transport of tracers. We take into account the contribution from turbulent eddies to the tracer transport that represents the Stokes drift in the upper cloud region, where static stability is larger compared to the lower troposphere and

away from the equator (latitudes between 10 and 60 degrees in both hemispheres). Based on the zonal momentum balance with diffusive closures for potential vorticity fluxes, our scaling arguments show TEM upward vertical motion in zones and downward motion in belts, resolving the apparent contradiction with the Eulerian mean flow found in observations.

The observed circulation is generated from the top down of the atmosphere in a "downward control" fashion, as also happens on Earth (Haynes et al., 1991). In Jupiter, the circulation is driven by eddy fluxes generated in the upper troposphere and closed in the deep atmosphere, likely in an Ekman layer with magnetohydrodynamic (MHD) drag. Our proposed circulation in Jupiter is consistent with the deep jet stream distribution inferred from Juno spacecraft observations (e.g., Kaspi et al., 2018). While we need to displace the MHD drag layer to shallower levels in the GCM for computational reasons (making it deeper leads to exponentially longer equilibration times), doing so still leads to a physically consistent closure of the circulation, with the Eulerian circulation extending downward along surfaces of constant specific angular momentum.

The impact of our results on explaining the global distribution of ammonia (NH_3) across Jupiter's troposphere still needs further investigation. To gain a comprehensive understanding of the distribution of ammonia (NH_3) in Jupiter's atmosphere, it is necessary to consider the impact of various physical processes, such as dynamical transport, sources (chemical products, evaporation of precipitates), and sinks (photochemical destruction, condensation). Observations from Juno (e.g., Li et al., 2017) show a plume of NH_3 in the tropics adjacent to bands of NH_3-poor air that appears to be sinking.

From the maps of the NH_3 mass distribution, Ingersoll et al. (2017) argue that there is a net upward transport of ammonia in Jupiter that needs to be resolved since there is no NH_3 rain or chemical reactions to close the NH_3 budget. Ingersoll et al. (2017) estimate that spherical NH_3 droplets with diameters 1-5 mm evaporate before reaching pressures deeper than 1-1.5 bar. Juno's microwave radiometer experiment (MWR) observed a change in microwave brightness gradient with depth. In Fletcher et al. (2021), it was found that belts change from being depleted to being enriched in NH_3 as a function of pressure. Levels with pressure values lower than 5 bar are depleted in NH_3 while levels with pressure values higher than 10 bar are enriched in NH_3. It has been suggested that a multi-tier circulation (Ingersoll et al., 2000; Showman and de Pater, 2005) may account for this observation, and also for the preferred lightning formation within the belts (Little et al., 1999; Gierasch et al., 2000; Porco et al., 2003). However, no physical mechanism has yet been proposed to close the circulation near cloud tops, which requires a change in the eddy momentum flux divergence that violates wave activity conservation. Also, like in Earth's extratropics, thunderstorms can occur occasionally in areas where air is sinking in the mean.

Our proposed TEM circulation with enhanced divergence in zones and convergence, or reduced divergence, in belts, offers an explanation for the observations from Voyager IRIS (Carlson et al., 1994), which found that belts are warmer than zones. Above the cloud layer, the warmer zones imply a change in the temperature gradient in the upper troposphere (Fletcher et al., 2020; Simon-Miller et al., 2006). From the thermal wind equation off the equator, we expect the zonal jets to weaken with altitude through the

upper troposphere, creating a vertical shear, which is consistent with the atmospheric structure we propose.

Our proposed theoretical arguments have been validated through 3D GCM simulations of Jupiter. These simulations qualitatively capture the main dynamical properties in Jupiter's troposphere. Similar to what is seen in observations, regions with higher concentrations of liquid ammonia (zones) experience upward vertical motion, while regions with lower concentrations of liquid ammonia (belts) experience downward vertical motion.

The circulation proposed in this study aligns with previous works by Schneider and Liu (2009) and Liu and Schneider (2010), emphasizing the importance of using complex 3D models to interpret observational data and robust physical arguments that, in particular, close the angular momentum balance to understand Jupiter's atmospheric circulation.

Acknowledgments. This research was supported by the NASA Outer Planets Research Program (Grant NNX10AQ05G), a David and Lucile Packard Fellowship and the Carlsberg Research Stays Grant (CF22-0011). We thank Colette Salyk for providing the zonal velocities and eddy momentum fluxes inferred from Cassini's observations.

References

Achterberg, R.K., Ingersoll, A.P., 1989. A normal-mode approach to Jovian atmospheric dynamics. Journal of Atmospheric Sciences 46, 2448–2462.

Adcroft, A., Hill, C., Campin, J.M., Marshall, J., Heimbach, P., 2004. Overview of the formulation and numerics of the mit gcm, in: Proceed-

483 ings of the ECMWF seminar series on Numerical Methods, Recent devel-
484 opments in numerical methods for atmosphere and ocean modelling, pp.
485 139–149.

486 Andrews, D.G., 1983. A finite-amplitude Eliassen-Palm theorem in isentropic
487 coordinates. J. Atmos. Sci. 40, 1877–1883.

488 Andrews, D.G., 1987. On the interpretation of the Eliassen-Palm flux diver-
489 gence. Quart. J. Roy. Meteor. Soc. 113, 323–338.

490 Andrews, D.G., Holton, J.R., Leovy, C.B., 1987. Middle Atmosphere Dy-
491 namics. volume 40 of *International Geophysics Series*. Academic Press.

492 Andrews, D.G., McIntyre, M.E., 1976. Planetary waves in horizontal and
493 vertical shear: The generalized Eliassen-Palm relation and the mean zonal
494 acceleration. J. Atmos. Sci. 33, 2031–2048.

495 Andrews, D.G., McIntyre, M.E., 1978. Generalized Eliassen-Palm and
496 Charney-Drazin theorems for waves on axisymmetric mean flows in com-
497 pressible atmospheres. J. Atmos. Sci. 35, 175–185.

498 Bretherton, F.P., 1966. Critical layer instability in baroclinic flows. Quart.
499 J. Roy. Meteor. Soc. 92, 325–334.

500 Carlson, B.E., Lacis, A.A., Rossow, W.B., 1994. Belt-zone variations in the
501 Jovian cloud structure. J. Geophys. Res. 99E, 14623–14658.

502 Corrsin, S., 1974. Limitations of gradient transport models in random walks
503 and in turbulence, in: Advances in Geophysics. Academic Press. volume
504 18A, pp. 25–60.

505 Dritschel, D.G., McIntyre, M.E., 2008. Multiple jets as PV staircases: The
506 Phillips effect and the resilience of eddy-transport barriers. J. Atmos. Sci.
507 65, 855–874.

508 Edmon, H.J., Hoskins, B.J., McIntyre, M.E., 1980. Eliassen-Palm cross sec-
509 tions for the troposphere. J. Atmos. Sci. 37, 2600–2616.

510 Fletcher, L.N., Kaspi, Y., Guillot, T., Showman, A.P., 2020. How Well Do
511 We Understand the Belt/Zone Circulation of Giant Planet Atmospheres?
512 Space Science Reviews 216, 30. 1907.01822.

513 Fletcher, L.N., Oyafuso, F.A., Allison, M., Ingersoll, A., Li, L., Kaspi, Y.,
514 Galanti, E., Wong, M.H., Orton, G.S., Duer, K., Zhang, Z., Li, C., Guillot,
515 T., Levin, S.M., Bolton, S., 2021. Jupiter's temperate belt/zone contrasts
516 revealed at depth by juno microwave observations. Journal of Geophysical
517 Research: Planets 126, e2021JE006858.

518 Fu, Q., Liou, K.N., 1993. Parameterization of the Radiative Properties of
519 Cirrus Clouds. Journal of Atmospheric Sciences 50, 2008–2025.

520 Gierasch, P.J., Conrath, B.J., Magalhães, J.A., 1986. Zonal mean properties
521 of Jupiter's upper troposphere from Voyager infrared observations. Icarus
522 67, 456–483.

523 Gierasch, P.J., Ingersoll, A.P., Banfield, D., Ewald, S.P., Helfenstein, P.,
524 Simon-Miller, A., Vasavada, A.R., Breneman, H.H., Senske, D.A., the
525 Galileo Imaging Team, 2000. Observation of moist convection in Jupiter's
526 atmosphere. Nature 403, 628–630.

Haynes, P.H., Marks, C.J., McIntyre, M.E., Shepherd, T.G., Shine, K.P., 1991. On the downward control of extratropical diabatic circulations by eddy-induced mean zonal forces. J. Atmos. Sci. 48, 651–679.

Held, I.M., 1999. The macroturbulence of the troposphere. Tellus 51A-B, 59–70.

Held, I.M., 2000. The general circulation of the atmosphere, in: Proc. Program in Geophysical Fluid Dynamics, Woods Hole Oceanographic Institution, Woods Hole, MA.

Held, I.M., Schneider, T., 1999. The surface branch of the zonally averaged mass transport circulation in the troposphere. J. Atmos. Sci. 56, 1688–1697.

Ingersoll, A.P., Adumitroaie, V., Allison, M.D., Atreya, S., Bellotti, A.A., Bolton, S.J., Brown, S.T., Gulkis, S., Janssen, M.A., Levin, S.M., Li, C., Li, L., Lunine, J.I., Orton, G.S., Oyafuso, F.A., Steffes, P.G., 2017. Implications of the ammonia distribution on Jupiter from 1 to 100 bars as measured by the Juno microwave radiometer. Geophysical Research Letters 44, 7676–7685.

Ingersoll, A.P., Beebe, R.F., Mitchell, J.L., Garneau, G.W., Yagi, G.M., Müller, J.P., 1981. Interaction of eddies and mean zonal flow on Jupiter as inferred from Voyager 1 and 2 images. J. Geophys. Res. 86, 8733–8743.

Ingersoll, A.P., Gierasch, P.J., Banfield, D., Vasavada, A.R., the Galileo Imaging Team, 2000. Moist convection as an energy source for the large-scale motions in Jupiter's atmosphere. Nature 403, 630–632.

Kaspi, Y., Galanti, E., Hubbard, W.B., Stevenson, D.J., Bolton, S.J., Iess, L., Guillot, T., Bloxham, J., Connerney, J.E.P., Cao, H., Durante, D., Folkner, W.M., Helled, R., Ingersoll, A.P., Levin, S.M., Lunine, J.I., Miguel, Y., Militzer, B., Parisi, M., Wahl, S.M., 2018. Jupiter's atmospheric jet streams extend thousands of kilometres deep. Nature 555, 223–226.

Koh, T.Y., Plumb, R.A., 2004. Isentropic zonal average formulation and the near-surface circulation. Quart. J. Roy. Meteor. Soc. 130, 1631–1654.

Li, C., Ingersoll, A., Janssen, M., Levin, S., Bolton, S., Adumitroaie, V., Allison, M., Arballo, J., Bellotti, A., Brown, S., Ewald, S., Jewell, L., Misra, S., Orton, G., Oyafuso, F., Steffes, P., Williamson, R., 2017. The distribution of ammonia on Jupiter from a preliminary inversion of Juno microwave radiometer data. Geophys. Res. Lett 44, 5317–5325.

Little, B., Anger, C.D., Ingersoll, A.P., Vasavada, A.R., Senske, D.A., Breneman, H.H., Borucki, W.J., et al., 1999. Galileo images of lightning on Jupiter. Icarus 142, 306–323.

Liu, J., Goldreich, P.M., Stevenson, D.J., 2008. Constraints on deep-seated zonal winds inside Jupiter and Saturn. Icarus 196, 653–664.

Liu, J., Schneider, T., 2010. Mechanisms of jet formation on the giant planets. J. Atmos. Sci. 67, 3652–3672.

Liu, J., Schneider, T., 2011. Convective generation of equatorial superrotation in planetary atmospheres. J. Atmos. Sci. 68, 2742–2756.

572 Liu, J., Schneider, T., Kaspi, Y., 2013. Predictions of thermal and gravita-
573 tional signals of Jupiter's deep zonal winds. Icarus 224, 114–125.

574 Marshall, J., Adcroft, A., Hill, C., Perelman, L., Heisey, C., 1997a. A finite-
575 volume, incompressible Navier Stokes model for studies of the ocean on
576 parallel computers. J. Geophys. Res. 102, 5753–5766.

577 Marshall, J., Hill, C., Perelman, L., Adcroft, A., 1997b. Hydrostatic, quasi-
578 hydrostatic, and nonhydrostatic ocean modeling. J. Geophys. Res. 102,
579 5733–5752.

580 Mendonça, J.M., Read, P.L., Wilson, C.F., Lee, C., 2015. A new, fast and
581 flexible radiative transfer method for Venus general circulation models.
582 Planet. Space Sci. 105, 80–93.

583 Moreno, F., Sedano, J., 1997. Radiative balance and dynamics in the
584 stratosphere of Jupiter: Results from a latitude-dependent aerosol heating
585 model. Icarus 130, 36–48.

586 Nikurashin, M., Vallis, G.K., Adcroft, A., 2013. Routes to energy dissipation
587 for geostrophic flows in the Southern Ocean. Nature Geosci. 6, 48–51.

588 Plumb, R.A., 1979. Eddy fluxes of conserved quantities by small-amplitude
589 waves. J. Atmos. Sci. 36, 1699–1704.

590 Plumb, R.A., Ferrari, R., 2005. Transformed eulerian-mean theory. I: Non-
591 quasigeostrophic theory for eddies on a zonal mean flow. J. Phys. Oceanogr.
592 35, 165–174.

Porco, C., West, R., McEwen, A., Del Genio, A., Ingersoll, A., Thomas, P., Squyres, S., Dones, L., Murray, C., Johnson, T., et al., 2003. Cassini imaging of Jupiter's atmosphere, satellites, and rings. Science 299, 1541–1547.

Read, P.L., Barstow, J., Charnay, B., Chelvaniththilan, S., Irwin, P.G.J., Knight, S., Lebonnois, S., Lewis, S.R., Mendonça, J., Montabone, L., 2016. Global energy budgets and 'Trenberth diagrams' for the climates of terrestrial and gas giant planets. Quarterly Journal of the Royal Meteorological Society 142, 703–720.

Read, P.L., Gierasch, P.J., Conrath, B.J., Simon-Miller, A., Fouchet, T., Yamazaki, Y.H., 2006. Mapping potential-vorticity dynamics on Jupiter. I. Zonal-mean circulation from Cassini and Voyager 1 data. Quart. J. Roy. Meteor. Soc. 132, 1577–1603.

Rhines, P.B., Holland, W.R., 1979. A theoretical discussion of eddy-driven mean flows. Dyn. Atmos. Oceans 3, 289–325.

Salyk, C., Ingersoll, A.P., Lorre, J., Vasavada, A., Del Genio, A.D., 2006. Interaction between eddies and mean flow in Jupiter's atmosphere: Analysis of Cassini imaging data. Icarus 185, 430–442.

Schneider, T., 2004. The tropopause and the thermal stratification in the extratropics of a dry atmosphere. J. Atmos. Sci. 61, 1317–1340.

Schneider, T., 2005. Zonal momentum balance, potential vorticity dynamics, and mass fluxes on near-surface isentropes. J. Atmos. Sci. 62, 1884–1900.

615 Schneider, T., Liu, J.J., 2009. Formation of jets and equatorial superrotation
616 on Jupiter. J. Atmos. Sci. 66, 579–601.

617 Schneider, T., Walker, C.C., 2006. Self-organization of atmospheric macro-
618 turbulence into critical states of weak nonlinear eddy–eddy interactions.
619 J. Atmos. Sci. 63, 1569–1586.

620 Showman, A.P., de Pater, I., 2005. Dynamical implications of Jupiter's tro-
621 pospheric ammonia abundance. Icarus 174, 192–204.

622 Simon-Miller, A.A., Conrath, B.J., Gierasch, P.J., Orton, G.S., Achterberg,
623 R.K., Flasar, F.M., Fisher, B.M., 2006. Jupiter's atmospheric tempera-
624 tures: From Voyager IRIS to Cassini CIRS. Icarus 180, 98–112.

625 Smith, B.A., Soderblom, L.A., Johnson, T.V., Ingersoll, A.P., Collins, S.A.,
626 Shoemaker, E.M., Hunt, G.E., Masursky, H., Carr, M.H., Davies, M.E.,
627 et al., 1979. The Jupiter system through the eyes of Voyager 1. Science
628 204, 951–972.

629 Taylor, G.I., 1915. Eddy motion in the atmosphere. Phil. Trans. R. Soc.
630 Lond. A 215, 1–23.

631 Tung, K.K., 1986. Nongeostrophic theory of zonally averaged circulation.
632 Part I: Formulation. J. Atmos. Sci. 43, 2600–2618.

633 Vallis, G.K., 2006. Atmospheric and Oceanic Fluid Dynamics: Fundamentals
634 and Large-Scale Circulation. Cambridge University Press, Cambridge, UK.

635 Vasavada, A.R., Showman, A.P., 2005. Jovian atmospheric dynamics: an
636 update after Galileo and Cassini. Rep. Prog. Phys. 68, 1935–1996.

West, R.A., Baines, K.H., Friedson, A.J., Banfield, D., Ragent, B., Taylor, F.W., 2004. Jovian clouds and haze, in: Bagenal, F., Dowling, T.E., McKinnon, W.B. (Eds.), Jupiter: The Planet, Satellites and Magnetosphere. Cambridge University Press, pp. 79–104.

West, R.A., Friedson, A.J., Appleby, J.F., 1992. Jovian large-scale stratospheric circulation. Icarus 100, 245–259.

Young, R., 2018. Simulating jupiter's weather layer: Accompanying data for parts i and ii.

Young, R.M.B., Read, P.L., Wang, Y., 2019a. Simulating Jupiter's weather layer. Part I: Jet spin-up in a dry atmosphere. Icarus 326, 225–252.

Young, R.M.B., Read, P.L., Wang, Y., 2019b. Simulating Jupiter's weather layer. Part II: Passive ammonia and water cycles. Icarus 326, 253–268.

Zuchowski, L.C., Read, P.L., Yamazaki, Y.H., Renno, N.O., 2009. A heat engine based moist convection parametrization for Jupiter. Planet. Space Sci. 57, 1525–1537.

Zuchowski, L.C., Yamazaki, Y.H., Read, P.L., 2009. Modeling Jupiter's cloud bands and decks: 2. Distribution and motion of condensates. Icarus 200, 563–573.

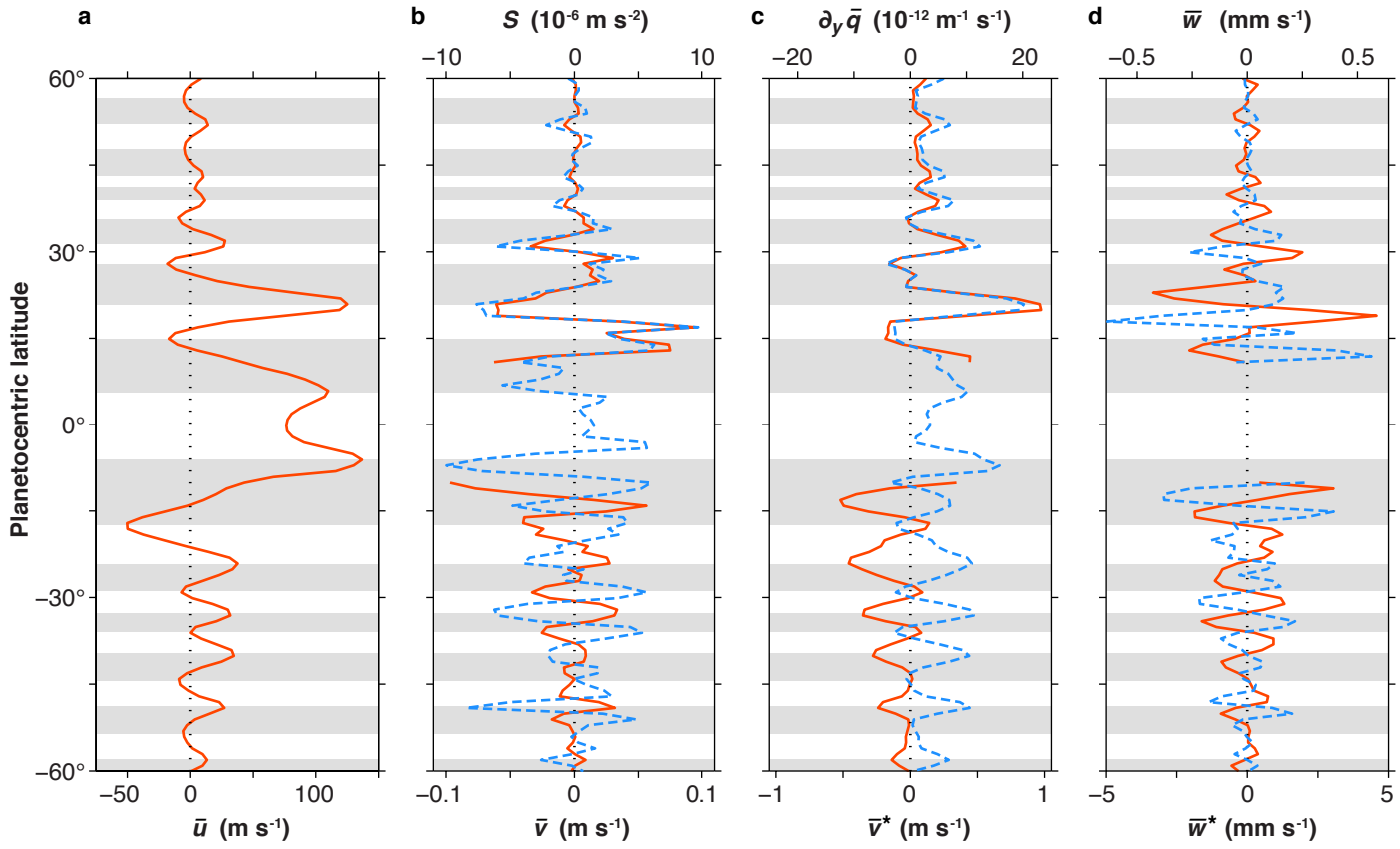

Figure 1: Zonal, meridional, and vertical velocities in Jupiter's upper troposphere. (a) Mean zonal velocity inferred from Cassini observations. (b) Eulerian mean meridional velocity (orange, lower axis) estimated as $\bar{v} \quad S{=}f$ from the eddy momentum flux divergence S (dashed blue, upper axis) inferred from Cassini observations. (c) Transformed Eulerian mean meridional velocity (orange, lower axis) estimated as $\bar{v}^* \quad (D{=}f)\partial_y\bar{q}$ ($D = 6 \quad 10^6\,\mathrm{m\,s^{-2}}$) from the approximate potential vorticity gradient $\partial_y\bar{q} \quad \partial_y(f + \bar{\ })$ (dashed blue, upper axis) implied by the zonal velocity in (a). (d) Eulerian mean (blue dashed, upper axis) and transformed Eulerian mean (orange, lower axis) vertical velocities estimated as $(\bar{w};\ \bar{w}^*) = (H{=}2)\,\mathrm{div}(\bar{v};\ \bar{v}^*)$. Estimated velocities are not shown within $10°$ latitude, where the underlying approximations become inaccurate. Grey-shaded regions mark belts (cyclonic shear zones), in which the structure of clouds and hazes indicates downwelling; white regions mark zones, in which the structure of clouds and hazes indicates upwelling. The observed mean zonal velocity and eddy momentum fluxes are from Salyk et al. (2006).

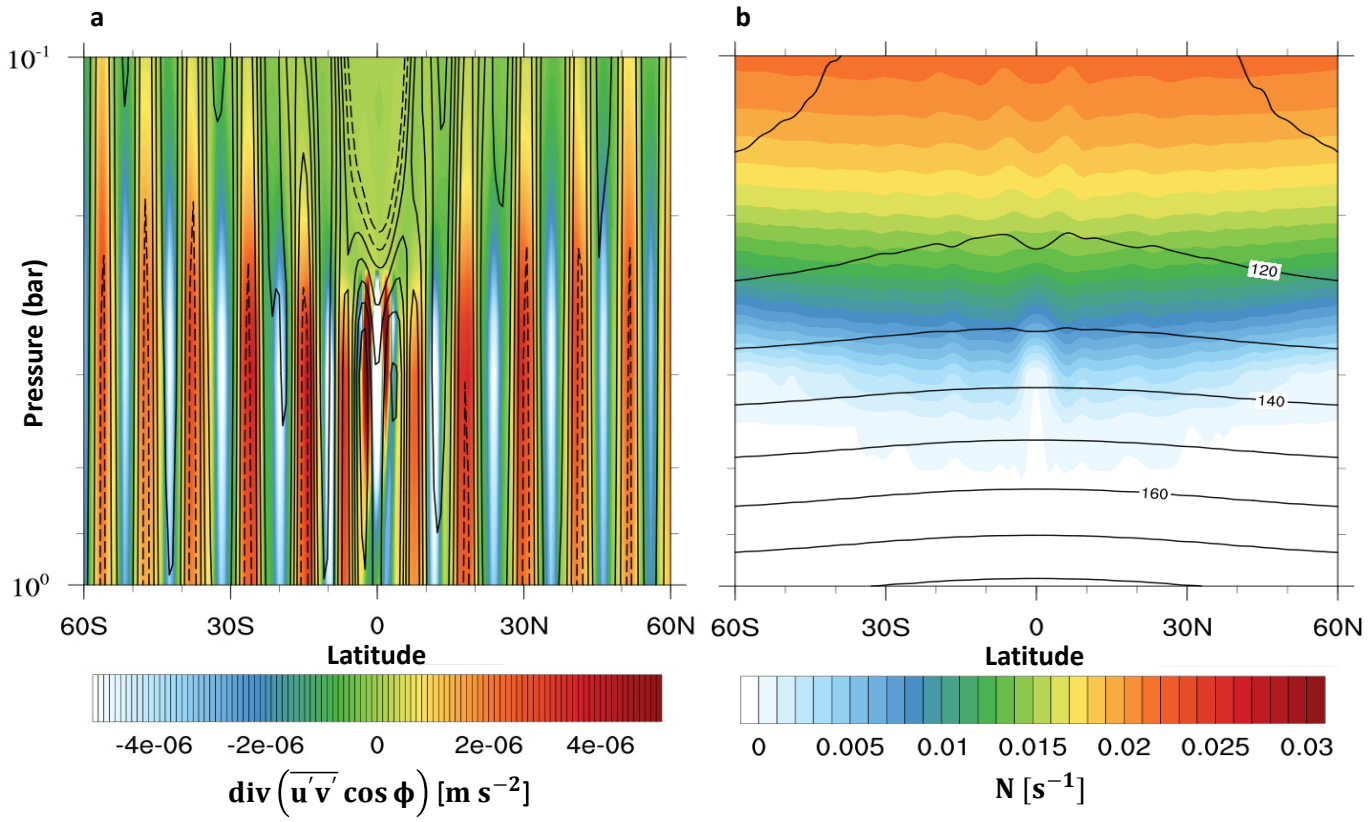

Figure 2: Mean flow fields in the latitude-pressure plane in the upper atmosphere of the simulation above 1 bar from Young et al. (2019a,b). (a) Zonal velocity (line contours) and horizontal eddy momentum flux divergence S (colours). The line contours represent zonal velocities between 8 and 28 $\mathrm{m\,s^{-1}}$, with a contour interval of 5 $\mathrm{m\,s^{-1}}$. Solid contours are for prograde flow, and dashed contours are for retrograde flow. (b) Temperature (contours, contour interval 10 K) and buoyancy frequency N (colours).

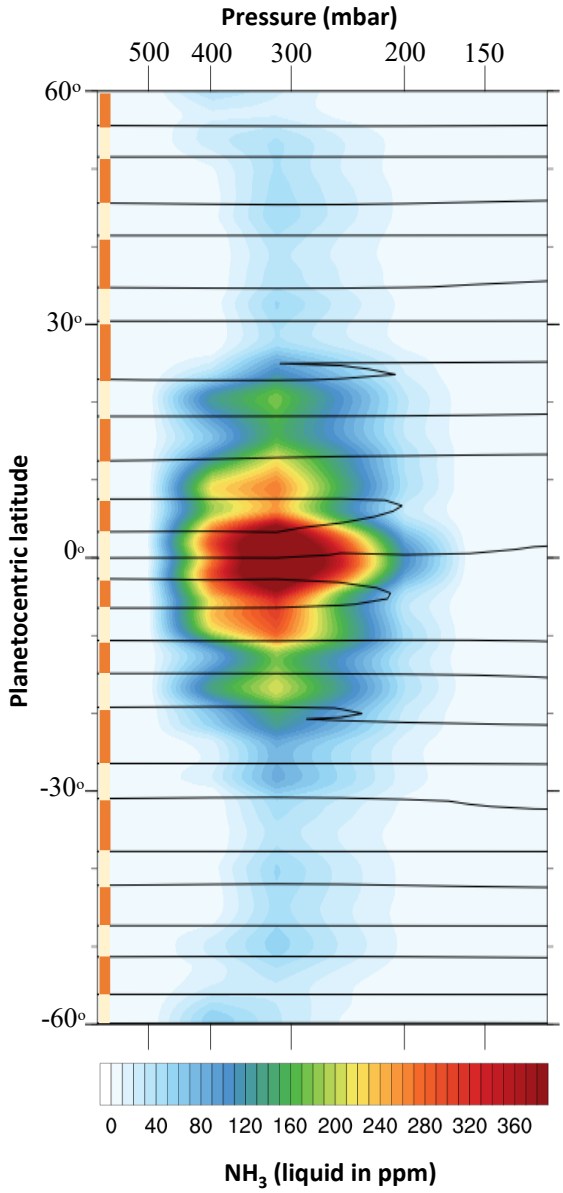

Figure 3: Latitude-pressure contour map representing the mass mixing ratio of liquid NH_3 in Jupiter's upper troposphere Young et al. (2019a,b). The GCM generates distinct zonal band patterns, which are closely linked to the pattern of the zonal winds. Belts are bands with low cloud density and cyclonic vorticity, while zones have higher cloud density and anticyclonic vorticity. The solid lines represent regions where the vorticity changes sign and the edges of the zonal band patterns. On the latitude axis, the thick orange lines represent the latitudinal extent of the belts (cyclonic shear zones), as in Fig. 1, and the thick white lines represent the zones (anticyclonic shear zones).

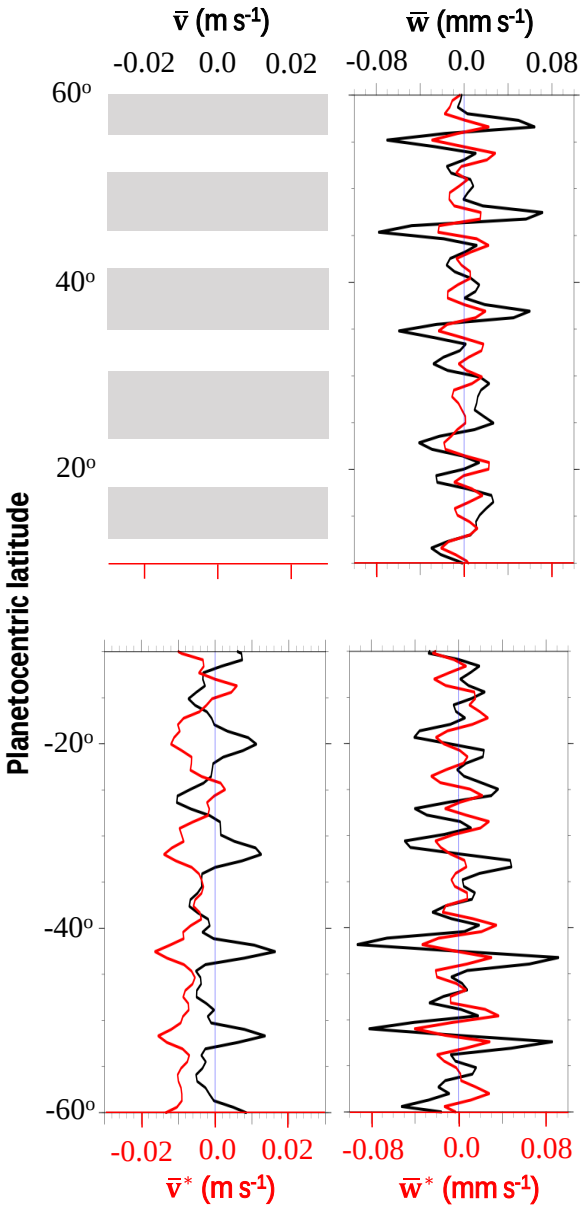

Figure 4: Simulated meridional and vertical velocities at Jupiter's NH_3 as a function of latitude (degrees) at 200 mbar. Grey-shaded regions mark belts (cyclonic shear zones), as in Fig. 1. The two left panels show the Eulerian mean meridional velocity (black line) and the transformed Eulerian mean meridional velocity (red line). Both meridional velocities are in units of m s^{-1}. The two right panels show the Eulerian mean vertical velocity (black line) and the transformed Eulerian mean vertical velocity (red line). Note that the vertical velocities in the GCM are in Pa s^{-1} and were converted to mm s^{-1} using the hydrostatic relation.